Title

Structural basis for tunable affinity and specificity of LxCxE-dependent protein interactions with the retinoblastoma protein family

Journal

Structure, 30(9)

ISSN

1359-0278

Authors

Putta, Sivasankar

Alvarez, Lucia

Lüdtke, Stephan

et al.

Publication Date

2022-09-01

DOI

10.1016/j.str.2022.05.019

Peer reviewed

HHS Public Access

Author manuscript

Structure. Author manuscript; available in PMC 2023 September 01.

Published in final edited form as:

Structure. 2022 September 01; 30(9): 1340–1353.e3. doi:10.1016/j.str.2022.05.019.

Structural basis for tunable affinity and specificity of LxCxE-dependent protein interactions with the retinoblastoma protein family

Sivasankar Putta[1], **Lucia Alvarez**[2], **Stephan Lüdtke**[3], **Peter Sehr**[4], **Gerd A. Müller**[1], **Samantha M. Fernandez**[1], **Sarvind Tripathi**[1], **Joe Lewis**[4], **Toby J. Gibson**[5], **Lucia B. Chemes**[2,*], **Seth M. Rubin**[1,*,†]

[1)]Department of Chemistry and Biochemistry, University of California, Santa Cruz, CA 95064

[2)]Instituto de Investigaciones Biotecnológicas (IIBiO-CONICET), Escuela de Bio y Nanotecnologías (EByN), Universidad Nacional de San Martín, Av. 25 de Mayo y Francia, CP1650 Buenos Aires, Argentina

[3)]Belyntic GmbH, Richard-Willstätter-Str. 11, 12489 Berlin, Germany

[4)]Chemical Biology Core Facility, European Molecular Biology Laboratory, Heidelberg 69117, Germany

[5)]Structural and Computational Biology Unit, European Molecular Biology Laboratory, Heidelberg 69117, Germany

Summary

The retinoblastoma protein (Rb) and its homologs p107 and p130 are critical regulators of gene expression during the cell cycle and are commonly inactivated in cancer. Rb proteins use their “pocket domain” to bind an LxCxE sequence motif in other proteins, many of which function with Rb proteins to co-regulate transcription. Here, we present binding data and crystal structures of the p107 pocket domain in complex with LxCxE peptides from the transcriptional co-repressor proteins HDAC1, ARID4A, and EID1. Our results explain why Rb and p107 have weaker affinity for cellular LxCxE proteins compared to the E7 protein from human papillomavirus, which has been used as the primary model for understanding LxCxE motif interactions. Our structural and mutagenesis data also identify and explain differences in Rb and p107 affinities for some

*Correspondence: lchemes@iib.unsam.edu.ar, srubin@ucsc.edu.
†Lead Contact: srubin@ucsc.edu

Author Contribution

Conceptualization and experimental design: L.B.C. and S.M.R. Sequence analysis: L.B.C. and T.J.G. Performance and experimental design of crystallization and ITC assays: S.P., S.M.F., and S.T. Preparation and design of peptide sequences and affinity data analysis: L.A. Peptide Synthesis: S.L. Peptide measurement using AlphaScreen assay: J.L and P.S. Cellular assay experimental design and performance: G.A.M. Manuscript drafting: S.P., S.M.R and L.B.C. Manuscript editing: S.P., L.A, G.A.M., T.J.G, L.B.C. and S.M.R.

Declaration of Interests

The authors declare no competing interests.

LxCxE-containing sequences. Our study provides new insights into how Rb proteins bind their cell partners with varying affinity and specificity.

Graphical Abstract

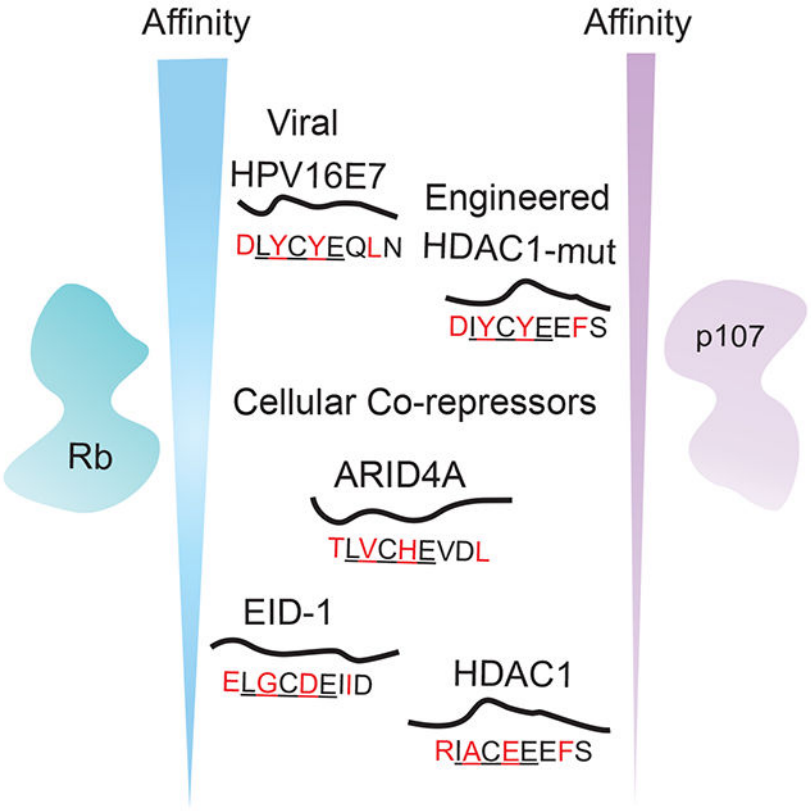

eTOC Blurb

The retinoblastoma (Rb) protein family regulates gene expression during the cell cycle through interactions with a number of transcriptional co-repressors. Putta et al. use X-ray crystallography and affinity measurements to understand how different cellular proteins use variations of an LxCxE motif to bind Rb proteins with different affinities and specificities.

Keywords

cell-cycle control; gene regulation; protein-protein interactions; short linear motif; tumor suppressor

Introduction

The Rb tumor suppressor protein is critical for normal development and is commonly found inactivated in cancer (Sherr and McCormick, 2002). Rb has numerous activities centered around regulation of cell-cycle dependent gene expression and genome maintenance (Burkhart and Sage, 2008; Dick and Rubin, 2013). In addition to its best-studied function

of inhibiting E2F transcription factors, Rb plays a role in genomic repeat silencing, cell lineage stability, DNA break repair, DNA replication, and formation of higher-order chromatin structures (Dick et al., 2018). Many of these functions are mediated by yet poorly understood protein interactions. Cells that lack Rb or contain Rb protein that is constitutively inactivated by upstream kinases or DNA tumor viral proteins are prone to genotoxic stress and transformation, and therapeutics that restore Rb activity are now being used to treat cancer (Knudsen et al., 2019).

Many Rb functions, for example negative regulation of cell-cycle progression and inhibition of E2F dependent transcription, are shared by two close paralogs p107 and p130 (p107/p130) (van den Heuvel and Dyson, 2008). Rb family proteins repress gene expression during quiescence and the G1-S transition by binding E2Fs, which inhibits E2F transactivation, and recruiting co-repressor proteins like HDAC1 (Histone deacetylase 1), EID1 (EP300-interacting inhibitor of differentiation 1), and ARID4A (AT-rich interaction domain-containing protein 4a) to E2F promoters (Dick and Rubin, 2013; Ferreira et al., 1998; Lai et al., 1999; MacLellan et al., 2000; Miyake et al., 2000). Despite these functional redundancies, Rb is found more commonly mutated in human cancer than p107 and p130, and loss of Rb is sufficient to promote tumorigenesis in mouse models (Classon and Harlow, 2002; Knudsen et al., 2019; Mulligan and Jacks, 1998). The molecular differences between Rb and its paralogs that account for the more potent tumor suppressor capacity of Rb are still incompletely understood. There is evidence that interactions with E2Fs vary (Liban et al., 2017; Liban et al., 2016; Trimarchi and Lees, 2002), and interactions with co-repressors have been better characterized for Rb, although it has been reported that p107 binds ARID4A and HDACs (Ferreira et al., 1998; Lai et al., 1999).

The Rb family proteins act as scaffolds that assemble diverse protein complexes in a manner that is regulated by multisite phosphorylation (Dick and Rubin, 2013; Morris and Dyson, 2001; Rubin, 2013). Therefore, determining molecular details for how Rb proteins interact with cellular partners is critical for understanding function and regulation of these important tumor suppressors. Rb proteins contain three primary functional domains: an N-terminal domain, a central “pocket” domain, and an intrinsically disordered C-terminal domain (Figure 1A) (Dick and Rubin, 2013). The loops that connect these domains and phosphorylation sites in the proteins mediate different conformations that control binding of more than 200 proteins (Morris and Dyson, 2001; Rubin, 2013; Sanidas et al., 2019). The structured pocket and N-terminal domains, which are well conserved in the family, each contain two tandem cyclin folds (A and B subdomains) that are connected by a disordered linker (Hassler et al., 2007; Lee et al., 1998). The pocket domain is necessary for nearly all Rb protein functions, including inhibition of E2F-dependent transcription (Dick and Rubin, 2013). The E2F transactivation domain binds at the interface between the A and B sub-domains (Lee et al., 2002; Xiao et al., 2003). The B subdomain contains the site that binds an LxCxE sequence motif present in many cellular and viral interacting proteins (Lee et al., 1998). Many functions outside of E2F association are mediated through the LxCxE cleft of the pocket proteins (Dick et al., 2018; Dick and Rubin, 2013). For example, the LxCxE-binding cleft is required for regulation of heterochromatin structures and proper mitotic condensation through recruitment of the condensin II complex (Coschi et al., 2010; Manning et al., 2010).

The LxCxE-cleft in the pocket domain is also used by Rb family proteins to regulate gene expression at E2F promoters. Interaction between an LxCxE-like motif in the protein LIN52 and p107 and p130 mediates formation of the DREAM complex, which represses cell cycle genes during quiescence (Guiley et al., 2015; Litovchick et al., 2011; Litovchick et al., 2007). In addition, transcriptional co-repressor proteins like HDAC1, ARID4A, and EID1 contain the LxCxE motif (Brehm et al., 1998; Defeo-Jones et al., 1991; Fattaey et al., 1993; Ferreira et al., 1998; Luo et al., 1998; MacLellan et al., 2000; Magnaghi-Jaulin et al., 1998; Miyake et al., 2000). Pocket proteins recruit the histone deacetylase HDAC1 to inhibit E2F-dependent transcription by modulating chromatin structure and the accessibility of co-activators and transcriptional machinery (Ferreira et al., 1998; Zhang et al., 2000). ARID4A (also known as Rb-binding protein 1 or RBP1) blocks E2F mediated gene transcription by forming complexes with Rb proteins, E2F, and HDAC1 at promoter sites and remodeling chromatin (Lai et al., 1999). The co-repressor EID1, which plays a role in promoting differentiation, binds to the Rb LxCxE cleft, and inhibits the histone acetyltransferase (HAT) activity of the co-activator protein p300 (MacLellan et al., 2000; Miyake et al., 2000). Although genetic ablation of the LxCxE-cleft in Rb results in normal cell growth and animal development, it leads to changes in chromatin structure, elevated cell-cycle gene expression, and increased cancer susceptibility in response to DNA damaging agents (Bourgo et al., 2011; Gonzalo et al., 2005; Talluri and Dick, 2012). These reports and bioinformatics analysis suggest the involvement of the LxCxE-cleft in binding a large set of proteins required for the regulation of cell functions (Kumar et al., 2021; Palopoli et al., 2018). The molecular basis of these interactions is, for the most part, unknown.

Several viral oncoproteins, including adenovirus E1A, SV40 T antigen (TAg), and human papillomavirus E7, also use LxCxE motifs to bind and suppress the function of Rb family proteins (DeCaprio, 2009; Kim et al., 2001; Lee et al., 1998; Palopoli et al., 2018). These motifs provide a required high affinity contact to Rb proteins (Chemes et al., 2010; Jones et al., 1990; Lee et al., 1998; Singh et al., 2005), which in conjunction with a second binding domain in the viral protein that directly competes with E2F, disrupts Rb protein-E2F complexes. Structural studies of E7 bound to Rb and p107, TAg bound to Rb, and the cellular protein LIN52 bound to p107 have revealed important details about the LxCxE-binding mode, including the key interaction made by the core leucine, cysteine, and glutamate residues (Guiley et al., 2015; Kim et al., 2001; Lee et al., 1998). In the case of LIN52, the central cysteine is replaced by a serine, and the resulting loss of affinity is compensated for by interactions with a phosphoserine that is C-terminal to the core motif. This sequence design creates a phosphoswitch that allows the interaction to be regulated by an upstream kinase and also makes association specific for p107/p130 over Rb (Guiley et al., 2015).

These observations regarding LIN52 association raise the questions of whether cellular LxCxE motifs generally bind Rb proteins with weaker affinity than E7 and other viral proteins and whether the relatively weak affinity is important for regulation. Differences in affinity between different LxCxE-containing proteins and the modulation of Rb binding by mutations to regions flanking the core motif also suggest that interactions beyond the core motif are critical for fine tuning of the LxCxE affinity (Jones et al., 1990; Palopoli et al., 2018; Singh et al., 2005). This idea is further motivated by a growing body of evidence

indicating that linear motif binding-affinity and specificity determinants are encoded by contextual features that include the wildcard positions, the residues flanking the core motif, and the conformation of the intrinsically disordered regions harboring the motifs (Bugge et al., 2020; Prestel et al., 2019). In the case of the LxCxE motif interaction with pocket proteins, limited structural knowledge, particularly of how cellular proteins bind, has limited our understanding of the key binding determinants. Here we present biophysical evidence that interactions between a large set of cellular LxCxE sequences, originally identified as Rb-binders, and pocket domains are weaker than interactions with the viral E7 motif and that several of these sequences bind Rb with higher affinity than p107. We report high-resolution structures of cellular HDAC1, ARID4A and EID1 LxCxE motif peptides bound to the human p107 pocket domain. The structures reveal additional determinants of peptide binding at the LxCxE site and the basis for higher Rb affinity, which we observed for some peptides. Our data reveal the mechanism for a fine-tuned interaction between LxCxE-containing proteins and Rb proteins that is balanced for affinity and regulation.

Results

Variation in affinities of cellular protein LxCxE sequences for Rb and p107

Previous measurements of binding affinities between LxCxE-containing peptides from HDAC1 and LIN52 for the Rb and p107 pocket domain demonstrate K_d values on the order of ~10 μM (Guiley et al., 2015; Singh et al., 2005), while the IxCxE motif from PRDM2 binds to Rb with ~0.6 μM affinity (Sun et al., 2015). These affinities are up to several hundred-fold weaker than for the LxCxE motif from the viral HPV16 E7 protein. In order to compare a larger sample of cellular proteins systematically using the same method, we performed an AlphaScreen assay to measure binding constants of several synthetic peptides containing LxCxE sequences from known Rb family interacting proteins (Figures 1B and S1 and Table S1). For this assay, we assembled a complex between a biotinylated peptide derived from the E7 LxCxE sequence and the pocket domains of either Rb or p107. The association was detected with streptavidin coated donor beads and nickel chelate- or glutathione-coated acceptor beads. The complex was then competed with untagged peptides corresponding to the sequences shown in Figure 1B, and the affinity of each sequence for Rb or p107 was calculated from concentration-dependent inhibition curves (Figure S1). We focused on LxCxE sequences from transcriptional co-repressor proteins (ARID4A, KDM5A, SMCA2, PRDM2, HDAC1, EID1, and BRG1) and proteins that regulate Rb phosphorylation (CycD paralogs from *Arabodopsis thaliana* were used for improved peptide synthesis). The results obtained with the AlphaScreen assay for HDAC1, PRDM2 and HPV16 E7 were in very good agreement with the previously measured affinities (Figure 1B) (Chemes et al., 2011; Singh et al., 2005; Sun et al., 2015).

Our results show that all the tested cellular LxCxE sequences bind to pocket proteins with weaker affinity than the HPV16 E7 peptide and present a wide range of affinities from K_d ~250 nM to ~100 μM. For many of the co-repressor proteins, binding of the peptides to the Rb pocket domain occurred with higher affinity than to the p107 pocket domain. We observe affinity differences up to 30-fold in the cases of ARID4A and PRDM2, whereas affinities are similar for all the CycD peptides and KDM5A. This observation suggests that some LxCxE

motifs are tuned for specific binding to Rb over p107, whereas other LxCxE-mediated interactions target both pocket proteins similarly. Our result is notable considering that the residues in the pocket cleft that contact the core residues in the LxCxE motif (LCE) are identical across Rb family proteins with a few exceptions that we explore below (Guiley et al., 2015; Lee et al., 1998). Overall, the affinity measurements performed here support the conclusion that subtle sequence differences outside the core LCE residues can greatly tune binding affinity. This conclusion is also supported by previous mutational studies and sequence analysis, which revealed the importance of the "χ" or "wild-card" positions, acidic residues in positions −1 to −3 from the core L residue, a stretch of acidic residues and/or phosphorylation sites located C-terminal to the core LxCxE motif, and a conserved hydrophobic residue located C-terminal to the LxCxE motif, often at the +2 position (Figure 1B) (Chemes et al., 2011; Chemes et al., 2010; Guiley et al., 2015; Jones et al., 1990; Kumar et al., 2021; Palopoli et al., 2018; Singh et al., 2005).

Crystal structures of the p107 pocket domain in complex with LxCxE peptides from transcriptional co-repressors

In order to understand the structural basis for how subtle sequence differences can influence LxCxE-protein affinity, we conducted x-ray crystallography studies on LxCxE peptides from cellular proteins in complex with the pocket domain. We selected the minimal regions of several cellular LxCxE motif peptides based on their similarity to the previously crystallized E7 peptide (Figure 1B, underlined sequences) (Lee et al., 1998). For the pocket domain we used a protein construct p107ΔL (residues 389–972, Δ600-779, Δ888-923), which contains the human p107 pocket domain sequence with two internal loops deleted. We were previously successful in solving structures of E7 and LIN52 peptides bound to the p107 pocket domain using this construct (Guiley et al., 2015), and we found we could reproducibly grow crystals in similar conditions with several LxCxE peptides. Crystals grown with p107ΔL pocket domain and human HDAC1, ARID4A, and EID1 LxCxE peptides diffracted to 2.6 Å, 2.7 Å, and 2.2 Å, respectively (Table 1, Figure 2, and Figure S2A). Structures were determined by molecular replacement using the p107ΔL pocket domain from the E7 complex structure (PDB: 4YOZ) as a search model. When bound to the HDAC1 or EID1 peptides, the p107 domain crystallized with one complex in the asymmetric unit in the $C2_1$ space group, while the ARID4A-p107ΔL complex crystallized with two copies in the P1 space group. As expected, all three peptides bind to the B subdomain at a site distinct from where the E2F transactivation domain binds (Figure 2B-2D). The pocket domain shows minimal differences among the structures and in comparison to the domain bound to the E7 LxCxE peptide (Figure S2B).

Cellular LxCxE peptide interactions beyond the core motif

The LxCxE peptides from the transcriptional co-repressor proteins all display similar interactions made by the alternating LCE residues as previously observed for the viral E7 and TAg sequences (Guiley et al., 2015; Kim et al., 2001; Lee et al., 1998) (Figure 3). Briefly, the leucine and cysteine insert into shallow hydrophobic pockets formed between the third and fifth helices of the B subdomain cyclin fold, and the glutamate sidechain makes backbone hydrogen bonds that cap the N-terminus of the fourth helix in the fold. While these interactions are invariant, we observe a number of interactions and structural features

that vary among the co-repressor protein peptides and are different from the mode of binding of the tighter affinity viral peptides. These include interactions N-terminal and C-terminal to the core LxCxE motif and the position and interactions of the wild-card sidechains.

Interactions N-terminal to the LxCxE motif—The viral E7 protein has an acidic aspartate at the −1 position relative to the start of the LxCxE motif, and an acidic residue is present in position −1 to −3 in all the other cellular peptides in our affinity study (Figure 1B). In some of the low affinity cellular peptides (e.g. HDAC1, SMCA2, and BRG1), there are positive charges N-terminal to the LxCxE motif. It was previously reported that replacing the N-terminal basic arginine residue at the −1 position in the HDAC1 peptide for an acidic aspartate residue (R413D) increased the affinity 2-fold and that mutation of the −1 aspartate in E7 (D21R) decreased affinity 5-fold for Rb, suggesting that interactions involving acidic residues at the −1 position may contribute mildly to stability (Singh et al., 2005). In the Rb-bound E7 (1GUX) structure, the acidic aspartate residue in the −1 position (D21) makes a long-distance hydrogen bond interaction with the χ^2 sidechain (Y25) of the E7 peptide (Figure 4A); however, the same D21 points away from Y25 in the structure of E7 bound to p107 (Figure 4B). The −1 position of the SV40 TAg LxCxE motif points away from the binding groove, but it is part of an alpha helix structure (Figure 4C). The cellular peptide we studied that contains a −1 acidic is EID1 (E177), and the structure shows a previously unobserved interaction made at this position. E177 makes a salt bridge with K853, and K853 is repositioned relative to the other structures such that an additional hydrogen bond is made with the E177 backbone carbonyl (Figure 4D). These results suggest that the positioning and interactions made by the acidic residues at the N-terminus of the motif can vary. The p107-bound EID1 structure also reveals an interaction made by an acidic residue in the −2 position (E176), which forms a salt bridge with K943 in p107 (Figure 3C and 4D). While the EID1 peptide N-terminus appears uniquely well ordered compared to other LxCxE peptides in structures with p107 and Rb, we note that there are packing interactions between EID1 and symmetry-related EID1 and p107 molecules in the crystal structure (Figure S3). It may be that these packing interactions stabilize the observed conformation of the EID1 peptide N-terminus.

To assess whether the structured acidic residues located at positions −1 and −2 of EID1 contributed stabilizing interactions, we measured by isothermal titration calorimetry (ITC) the binding affinity of an EID1 peptide in which we mutated the −1 and −2 glutamates to arginine (E176R/E177R). This mutation did not result in a significant loss of EID1 peptide affinity for Rb or p107 (Table 2, Figures S4A-S4D). We also tested affinity of the wild-type EID1 peptide for both pocket domains in which the two lysines interacting with the N-terminal glutamates were mutated to alanine. These mutations resulted in loss of binding in the ITC experiment, while a control peptide corresponding to the E2F4 transactivation domain still bound the mutated domains (Table 2, Figures S4E-S4H). Lysine K853 in p107 makes a hydrogen bond with the backbone of the EID1 peptide in the crystal structure of the EID1-p107 complex, which may explain why mutation on the pocket domain side had an effect, whereas mutation of the peptide did not significantly change affinity. We conclude that there is no evidence supporting an influence of the −1 and −2 glutamates on EID1 affinity.

An acidic residue is present in position −2 in ARID4A and in position −3 in LIN52, for which there are now structures available. However, the N-terminal acidic residues are not visible in the electron density in those structures. We could only build the ARID4A peptide in the structure solved here starting at L957, which is the canonical Leu in the motif (Figure 3B). We tested using ITC binding of an ARID4A peptide containing a mutation of the −2 sidechain (E955R) and found a 3.5-fold loss of affinity for Rb, but no significant loss of affinity for p107 (Table 2, Fig. S4I-S4L). Together our observations suggest that well-ordered salt bridge interactions are not generally observable between acidic residues N-terminal to the LxCxE motif and lysines that are near the pocket domain binding cleft. Furthermore, mutation of these residues near cellular LxCxE sequences either does not lead to significant changes in affinity or, in some cases, produces mild effects (2-5 fold) on peptide association with Rb (Table 2 and (Singh et al., 2005)).

Wild-card residues of the LxCxE motif—Based on the E7 structure and mutagenesis data, it has been suggested that the affinity of LxCxE-sequences depends on the identity of the residues in the “wild-card” positions, even though these residues point away from the pocket domain (Jones et al., 1990; Palopoli et al., 2018; Singh et al., 2005). Our binding data support the hypothesis that bulky aromatic and perhaps to a lesser extent aliphatic sidechains in the wild-card spots confers higher affinity. For example, EID1, which has a glycine and aspartate in χ^1 and χ^2 (G,D), HDAC1 (A,E), and SMCA2 (T, E) all have affinities ~10 μM or greater. In contrast, ARID4A (V, H) and KMD5A (F, D) have affinities ~1 μM, and the viral E7 peptide (Y, Y) has submicromolar affinity.

The structures suggest two potential explanations for the increase in affinity conferred by bulky sidechains in the wild-card positions. In the Rb-bound E7 structure, the tyrosines at χ^1 and χ^2 are positioned to make stacking interactions (Figure 4A), demonstrating that large sidechains are able to contact each other for van der Waals interactions. In the case of p107-bound E7, however, the Y23 (χ^1 position) is instead pointing toward and contacts V939 in p107, which is not conserved in Rb (M761) (Figure 4B). The Y25 (χ^2 position) is still aligned in the p107 structure with its position in the Rb structure, sitting just above the backbone amide nitrogen and carbonyl of C24. Notably, in the structure of ARID4A determined here, H960 in the χ^2 position also adopts the same x2 conformation, bringing it close to V958 (χ^1 position in ARID4A) for van der Waals contacts and covering the C959 backbone nitrogen and carbonyl (Figure 4F). In all the solved LxCxE peptide structures, these cysteine backbone atoms form a bidentate hydrogen bond with the conserved N935 asparagine sidechain in the p107 pocket domain (N757 in Rb). The invariance of the χ^2 sidechain orientation, also observed for D181 in EID1 (Figure 4D), suggests the additional role of shielding this critical hydrogen bond from water. We found that mutation of N935A in p107 and N757A in Rb results in complete loss of detectable association by ITC for the high affinity E7 peptide, yet in control experiments to ensure the pocket structure is intact, the asparagine mutants still bind the E2F4 transactivation domain (Table 2 and Figures S4M-S4R). These data support the idea that the hydrogen bond interactions made by the asparagine are critical determinants required for LxCxE motif binding to the pocket domain. We propose that the peptides with bulkier χ^2 amino acids are more effective at shielding and bind with higher affinity. However, considering that bulky amino acids in the χ^2 position

also have greater potential to make an intramolecular interaction with the χ^1 sidechain, as in the Rb-E7 and p107-ARID4A complexes, our structural and binding data alone cannot distinguish between the two mechanisms by which bulky wildcard residues may enhance affinity.

Interactions C-terminal to the core LxCxE motif—It has been known from viral peptide structures and the LIN52 structure that a sidechain C-terminal to the LxCxE core motif fills a shallow hydrophobic pocket formed by the fourth and fifth cyclin fold helices and the intervening linker in the pocket domain (Guiley et al., 2015; Kim et al., 2001; Lee et al., 1998). In these previous structures, the residue filling that pocket is a leucine in the +2 position (or +2 methionine in the case of the SV40 T antigen). All the peptides in our binding studies have either a +2 or +3 hydrophobic residue, except notably SMCA2, mmBRG1, CycD1 and CycD2, which all have relatively weak affinity and harbor hydrophobic residues at +4 or +5 (Figure 1B). This comparison suggests that the +2/+3 hydrophobic interactions are important for high affinity, a conclusion also supported by mutagenesis of the HDAC1 sequence (Singh et al., 2005).

Comparison of previous structures and the structures determined here reveals how the pocket can accommodate bulkier hydrophobic sidechains and a hydrophobic sidechain at the +3 position. This hydrophobic pocket is rather wide and shallow, and even the E7 (+2 Leu), LIN52 (+2 Leu) and EID1 (+2 Ile) peptides with similar amino acids in the +2 position fill the pocket with slightly different positions of the sidechain (Figure 5A). Another feature of the hydrophobic pocket is the pliability of M865 in p107, which forms the pocket base on the side near the fourth helix of the cyclin fold. In the HDAC1 structure, a bulkier phenylalanine in the +2 position (F420) is inserted deeper into the pocket, and the M865 sidechain changes its position to accommodate F420 (Figure 5B). An alternative M865 conformation is also observed in the ARID4A structure, which has a +3 Leu (L964). To accommodate the extra residue, the ARID4A main chain bulges out following the canonical E position (E961) and then approaches the hydrophobic pocket in p107 at a steeper angle. This results in the deeper insertion of L964 compared to the same side chain at the +2 position in other peptides, and L964 can be accommodated because M865 is again repositioned (Figure 5C).

The sequences C-terminal to the LxCxE motif in both the cellular and viral proteins have a number of acidic residues (Figure 1B), and truncation of these residues from peptides has been shown to weaken affinity (Chemes et al., 2011; Chemes et al., 2010; Palopoli et al., 2018; Singh et al., 2005). Addition of negative charge through phosphorylation has also been shown to increase affinity (Chemes et al., 2011; Chemes et al., 2010; Guiley et al., 2015; Palopoli et al., 2018; Pflum et al., 2001). In the case of LIN52, the structure shows the phosphoserine coordinated by a set of p107 pocket domain residues including two arginines (R869 and R880) that are conserved in Rb (Guiley et al., 2015). In contrast, we have found in these crystal structures that the C-terminal acidic residues either do not show ordered electron density (HDAC1), or they do not form any specific interactions with basic sidechains (ARID4A and EID1). The absence of ordered interactions may be due to the known diffuse long-range electrostatic interactions that drive the affinity (Chemes et al., 2011), which may be favored by a high degree of disorder in this region.

Origin of higher affinity of Rb for several cellular LxCxE peptides

It is notable that the M865 position is not conserved in Rb, which has a valine at this position (V725) (Figure 5D). We hypothesize that the deeper pocket created by the shorter valine sidechain is a source of the higher affinity of several peptides for Rb (Figure 1B). We observed that the M865 orientation changes relative to the E7-p107 structure when p107 is bound with a peptide containing a bulky +2 phenylalanine (HDAC1, Figure 5B) or +3 hydrophobic sidechain (ARID4A, Figure 5C). This observation suggests that some peptides bind p107 weaker because they do not deeply bury the hydrophobic sidechain at the +2/+3 position or there is an energetic cost in repositioning M865. To test whether the presence of an Rb-like valine at the M865 in p107 confers higher affinity, we purified a p107 pocket domain harboring an M865V mutation and tested binding to the ARID4A peptide by ITC (Figure 5E). The affinities of ARID4A for wild-type Rb and p107 pocket domains were similar albeit slightly tighter than the affinities we measured by AlphaScreen. Notably, data from both techniques demonstrate that ARID4A has a 10- to 30-fold greater affinity for Rb over p107 that we hypothesize arises from the requisite deep insertion of the +3 Leu into the hydrophobic pocket with the V725/M865 floor. We found in the ITC assay that the M865V p107 mutant binds the ARID4A peptide with ~13-fold greater affinity compared to wild-type p107 and with an affinity that is similar to its affinity for Rb (Table 2 and Figure 5).

The second sequence difference that may account for why some LxCxE motif peptides bind stronger to Rb is the presence of M761 in Rb compared to V939 in p107. Here, the longer M761 sidechain can make closer contact with the canonical Leu and χ^1 sidechains in the motif as well as the peptide backbone (Figure 4). We found that a V939M p107 pocket domain mutant binds the ARID4A peptide with ~5-fold tighter affinity than wild-type p107 (Table 2 and Figure S4S), supporting the importance of the sidechain at this position. However, it is not clear why binding of some peptides, like ARID4A, is more affected by this substitution compared to other peptides (e.g. E7), which have similar affinity for Rb and p107. A contributing factor may be that the longer M761 sidechain in Rb pushes the χ^1 sidechain position toward the χ^2 sidechain, which better covers the N757 hydrogen bonds (compare Figures 4A and 4B). This distinction may explain why the same Y23 at the χ^1 position in E7 adopts a different orientation when bound to Rb or p107. The orientation of the χ^1 phenylalanine in SV40 when bound to Rb similarly points toward the χ^2 sidechain (Figure 4C). Together these observations suggest that differences in χ^1 and χ^2 sidechain rotamer conformations may be imparted by the M761/V939 substitution.

An engineered high affinity LxCxE-motif promotes association of HDAC1 with pocket proteins

We next introduced mutations into the HDAC1 sequence in order to engineer a higher affinity sequence. Based on our structural analysis and binding data (Singh et al., 2005), we chose mutations at the −1 position (R413D) and the wild card positions (A415Y, E417Y) that mimic the viral E7 LxCxE motif. We found using ITC that whereas the titration of p107 with the wild-type HDAC1 peptide yields poor signals and barely saturates using our conditions (we estimate $K_d > 10$ μM), the HDAC1 triple (3X) mutant peptide has affinity $K_d = 105 \pm 5$ nM (Figure 6A and Table 2). The HDAC1 mutant peptide also binds Rb tightly

(Figure S4T), and we similarly observed that mutation of the wild-card residues in EID1 to tyrosines results in higher affinity for both Rb and p107 (Table 2 and Figures S4U-S4V). We determined the crystal structure of the HDAC1 3X mutant peptide bound to p107 and found that the tyrosines added to the wild-card positions are oriented similar to their position in the E7 peptide structure (Figure 6B). Y417 covers the backbone of C416 and Y415 is rotated toward V939. The D413 added to the −1 position makes the hydrogen bond interaction with the Y415 in the χ^2 position observed in the Rb-bound E7 structure (Figure 6B). Overall, the conformation of the HDAC1 mutant peptide resembles more the structure of E7, which is consistent with the higher observed affinity and supports the conclusion that the orientation of bulky wild card residues is an important source of high affinity. To test the effects of a high affinity HDAC1 interaction in cells, we expressed Flag-tagged wild-type and mutant HDAC1 in HCT116 cells and assayed co-immunoprecipitation of endogenous Rb and p107. We tested the R413D, A415Y, and E417Y mutations individually and in combination. We performed the experiment in cells with either palbociclib or nocodazole treatment, which arrests cells in G1 with pocket proteins hypophosphorylated or in mitosis with pocket proteins hyperphosphorylated, respectively. We found that the triple HDAC1 mutant in particular more robustly associates with Rb and p107 when cells are arrested in G1 (Figure 6C). In the nocodazole treated cells, we do not see a comparable increase in phosphorylated Rb or total p107 binding to the high-affinity HDAC1 mutant, suggesting that the effects of phosphorylation are still sufficient to dissociate pocket protein from the LxCxE motif. We note that we still observe an increase in band intensity when probing for total Rb in the immunoprecipitation from nocodazole cells, which, considering the result with the phosphospecific antibody, is most likely due to the presence of residual hypophosphorylated Rb.

Discussion

While it has been shown that many cellular and viral proteins bind to Rb pocket proteins utilizing an LxCxE motif, there has been little systematic analysis of the sequence and structural features that are critical for determining affinity. Here we present biochemical and structural data that further enhance our understanding of these determinants, particularly in the context of transcriptional co-repressor proteins that bind with LxCxE motifs. While more systematic mutagenesis of viral and cellular LxCxE sequences will be required to build a high-resolution map of LxCxE affinity and specificity, our results demonstrate that sequence determinants of both the LxCxE motifs and the Rb/p107 binding clefts encode the affinity and specificity of cellular interactions. By determining the binding affinities of a set of cellular LxCxE sequences, we demonstrate that host LxCxE motifs bind to pocket proteins with lower affinity than the prototypical viral E7 motif. We also show that host interactions present a wide range of affinities, and that fine tuning of the LxCxE motif sequence can lead to similar (EID1, KDM5A, CycD) or different (HDAC1, ARID4A, PRDM2, SMCA2/BRG1) affinities for Rb and p107. Beyond the core, LCE residues, the most important sequence features contributing to the binding affinity and specificity include the identity of the χ^1 and χ^2 residues and a hydrophobic sidechain at the +2/+3 position following the motif. Notably, these important determinants are often poorly optimized in the cellular proteins. Our results also provide structural explanations for several of these effects,

for example, the possible protection of the N935 hydrogen bonds by bulky sidechains in the wild-card positions and the capacity of the +2/+3 sidechain to be deeply buried in a hydrophobic pocket. This latter interaction confers higher affinity for Rb in the case of some peptides, because Rb harbors a smaller sidechain (V725) at the base of this pocket compared to p107 (M865). These design principles could be used in future efforts to synthesize viral-pocket protein inhibitors (Fera et al., 2012).

Our results provide insights into how the affinity and specificity of LxCxE-pocket protein interactions are encoded. Fine tuning of the motif sequence can produce short linear motifs (SLiMs) with binding affinities that range from nanomolar (viral E7 motif) to micromolar (cellular motifs). By performing site-directed mutagenesis of the Rb/p107 clefts we also show how single substitutions in these clefts can determine binding specificity towards Rb versus p107 for some cellular motifs. Our results exemplify how affinity and specificity are encoded by both the disordered LxCxE motif sequence and its ordered binding cleft, as shown for other SLiM-domain interactions (Ivarsson and Jemth, 2019). This suggests that both binding partners have been tuned throughout evolution to produce interactions that are shared between pocket proteins, and interactions that are specific towards Rb (ARID4A) or p107/p130 (LIN52). The broad range of affinities and specificities found in this system helps explain the large interaction potential of pocket proteins and exemplifies how highly specific interactions can evolve in intrinsically disordered regions (Teilum et al., 2021), a process aided by the higher evolutionary plasticity of SLiMs (Davey et al., 2015).

It remains an interesting question why viral proteins such as E7 have evolved to bind pocket proteins with high affinity, whereas cellular protein LxCxE motifs are often less optimized. In the case of viral proteins, very tight affinity may be required to target the pocket proteins early following infection or in differentiated epithelia, when viral effector protein concentrations are low (Banerjee et al., 2006; Crisostomo et al., 2019; Dowhanick et al., 1995). For cellular proteins, one possibility is that a weaker affinity may be needed for proper regulation of pocket protein interactions with functional partners. For example, the interactions of co-repressor proteins with Rb occur when Rb is hypohosphorylated, which is during G0/G1, and evidence suggests that specific phosphorylation events induce conformational changes that can disrupt binding to the LxCxE cleft (Burke et al., 2012; Ferreira et al., 1998; Harbour et al., 1999; Lai et al., 1999; Rubin, 2013). The idea that weak binding of an LxCxE motif better facilitates regulation has also been observed in the case of LIN52 binding to p107. The substitution of serine at the canonical cysteine position reduces binding, but phosphorylation of a C-terminal serine makes the association tighter (Guiley et al., 2015). We considered that cellular protein affinities are tuned such that they bind pocket proteins only when they are hypophosphorylated in the early cell cycle. However, we found that Rb and p107 phosphorylation is sufficient to dissociate the LxCxE-containing HDAC1 protein, even when the sequence is optimized to bind with high affinity similar to viral proteins. An alternative requirement for weak binding may be that it is needed for pocket proteins to form diverse complexes with a large pool of potential interacting partners, which can be switched through phosphoregulation or other molecular signaling events. SLiMs are commonly found to have micromolar affinity, as they often make multivalent interactions and utilize cooperativity for signaling (Gibson, 2009; Kumar et al., 2021). In fact, CycD, HDAC1, and EID1 are all known to make multivalent interactions with Rb proteins (Hassler

et al., 2007; MacLellan et al., 2000; Magnaghi-Jaulin et al., 1998; Miyake et al., 2000; Topacio et al., 2019).

A longstanding question about the pocket protein family is why Rb specifically has more potent tumor suppressor activity and is more often found mutated in cancer. One hypothesis is that subtle sequence differences between Rb, p107, and p130 account for different protein interactions that may mediate Rb-specific functions in suppressing growth or maintaining genomic integrity. Indeed, Rb was shown to specifically bind the activator E2Fs with high affinity, while only p107 and p130 are capable of binding LIN52 to assemble the DREAM complex (Guiley et al., 2015; Liban et al., 2017; Liban et al., 2016 ; Litovchick et al., 2007). Given the overall similarity of residues that form the LxCxE-binding cleft and observations of pocket protein associations with similar viral and cellular proteins containing the motif, it has been assumed that LxCxE-binding is a conserved function. In contrast, our results here suggest that Rb makes tighter interactions with several LxCxE peptides. It is possible that these LxCxE-binding differences also contribute to differences in tumor suppressor potency. Notably, mutation of the LxCxE-cleft promotes tumorigenesis *in vivo* and has been linked to defects in genome stability and chromatin condensation (Coschi et al., 2010). Additional study of functional differences between pocket proteins that arise from different LxCxE-interactions, for example with transcriptional co-repressors, may reveal other key mechanisms of Rb tumor suppression.

STAR Methods

Resource Availability

Lead contact—Further information and requests for resources and reagents should be directed to and will be fulfilled by the lead contact, Seth Rubin (srubin@ucsc.edu).

Materials availability—Plasmids generated in this study are available from the lead contact.

Data and code availability—X-ray diffraction data have been deposited in the Protein Data Bank and are publicly available as of the date of publication. Accession numbers are listed in Table 1 and the key resources table. This paper does not report original code. Any additional information required to reanalyze the data reported in this paper is available from the lead contact upon request.

Experimental Model and Subject Details

HCT116 colon carcinoma cells (ATCC CCL-247; isolated from adult male) were grown in Dulbecco's modified Eagle's medium (Gibco, high glucose, GlutaMAX Supplement, pyruvate) supplemented with 10 % fetal bovine serum (Corning, Regular Fetal Bovine Serum) and penicillin/streptomycin (Gibco). Cells were maintained at 37° C and 5 % CO_2.

Method Details

Generation of recombinant protein reagents—A GST fusion protein of the p107ΔL pocket domain (E389–Q972, ΔT600-779, Δ888-923) was expressed and purified from

BL21(DE3) *E. coli* cells similar to as previously described (Guiley et al., 2015). The culture, induced with 1 mM IPTG, was further grown for 15 hours at 18°C. Cells were harvested by centrifugation at 4000 rpm for 20 mins at 4°C. The cell pellets were lysed, and GS4B affinity chromatography was performed in 20 mM Tris (pH 8.0), 250 mM NaCl, 5 % Glycerol, 5 mM DTT and 1 mM PMSF. The GS4B purified protein was then subjected to GST-TEV protease cleavage and dialyzed overnight in 25 mM Tris, 250 mM NaCl, 5 mM DTT. The protein was then passed over GS4B affinity resin again to remove free GST and GST-TEV. Finally, the protein samples were concentrated and injected into a Superdex 75 Prep Grade column (Citvia) in a buffer containing 20 mM Tris (pH 8.0), 500 mM NaCl, 5 mM DTT. For ITC, a similar construct of the human Rb pocket domain lacking the single internal loop (residues 380-787; Δ582-642) was expressed and purified using the same protocol. For the AlphaScreen measurements, His-tagged Rb pocket domain was produced as previously described (Chemes et al., 2010). The His-tagged construct was expressed in Bl21(DE3)pLysS *E. coli* cells by addition of 1 mM IPTG at 28°C. Soluble protein was purified using Ni^{2+}-nitrilotriacetic acid immobilized metal affinity chromatography, cation exchange (SP-Sepharose), and Superdex 75 gel filtration. Mutant proteins were expressed from plasmids modified using site-directed mutagenesis and the oligonucleotides listed in Table S2.

X-ray crystallography—p107ΔL protein was crystallized following size-exclusion chromatography in complex with HDAC1, HDAC3X, ARID4A and EID1 peptides by the hanging drop method at 4 °C. Peptides were added in twofold molar excess to 20 mg/mL p107ΔL and incubated for 30 min on ice before the crystallization. The reservoir crystallization solution consisted of 100 mM MES (pH 6.5), 1.6 M $(NH_4)_2SO_4$, and 4% PEG 400. Crystals were flash frozen in the reservoir solution with 10 % glycerol. Data were collected at the Advanced Photon Source Beamline 23-D at 100K. Diffraction data from the ARID4A-p107ΔL crystals were indexed, integrated, and scaled using XDS (Kabsch, 2010). The data from the other peptide-p107ΔL complex crystals were processed by using XIA2 (Winter, 2010) and AIMLESS (Evans, 2006) in the CCP4 program suite (Winn et al., 2011). ARID4A and HDAC1-3X crystallized with p107ΔL in P1, and EID1 and HDAC1 crystallized with p107ΔL in $C2_1$ space group. Structure determination of these complexes was achieved by using molecular replacement with MOLREP and PDB ID: 4YOZ (E7-p107ΔL) as a search model (Vagin and Teplyakov, 2010). Alternative cycles of model building by COOT (Emsley and Cowtan, 2004) and refinement with Phenix (Adams et al., 2010) were applied to complete the structures (Table 1).

Peptide synthesis—Peptides for the AlphaScreen assay were provided by Belyntic GmbH. The peptides were purified by Belyntic's Peptide Easy Clean (PEC) technology using a reductively cleavable linker system (PEC linker RC+) following the solid phase peptide synthesis (SPPS) adapted to plate format using an automated parallel peptide synthesizer (Intavis MultiPep RSi) (Zitterbart et al., 2021). The purified peptides were obtained as TFA salts in solid form in a 96 well collection plate. Identity and purity of the peptides was confirmed by UPLC-ESI-MS. For all the peptides except atCCD1, atCCD2, and the HPV16E7, a tyrosine was added to the N-terminus of the sequence shown in Figure 1B in order to quantify peptide concentration. An N-terminal alanine was added to

atCCD21 to maintain five residues before the LxCxE motif and to HPV16E7 to replace the natural glutamine, and the C-terminal leucine in SMCA2 was replaced with a phenylalanine. Peptides for x-ray crystallography were synthesized by GenScript Biotech.

AlphaScreen assay—An AlphaScreen™ assay was used to measure the inhibition of the interaction between a biotinylated E7-peptide (Biotin-QPETTDLYSYEQLNDS) and the human Rb or p107 pocket domains produced with an N-terminal 6xHis-tag (Rb) or an N-terminal GST-tag (p107). The E7 sequence was synthesized as a 16-mer peptide with C→S replacement and functionalized on the N-terminus with biotin. Binding of the biotin-E7 peptide to His-tagged Rb or GST-tagged p107 was detected with Streptavidin-coated donor beads and nickel chelate- or glutathione-coated acceptor beads. Concentration-response curves of inhibiting peptides were generated from 11- fold 1:3 serial dilutions starting at 100 μM with 6 nM His-Rb or GST-107, 6 nM biotin-E7 peptide and equal concentrations of 5 μg/mL acceptor and donor beads in 15 μl final assay volume. The assay was performed in white 384-well ProxiPlates and PBS supplemented with 2 mM DTT, 0.05% Tween 20 and 0.1% BSA as buffer. The AlphaScreen signal was measured in an Envision plate reader (Perkin Elmer, United States of America). Equilibrium dissociation constants from the AlphaScreen assay were obtained by fitting the normalized data and considering the binding equilibrium of both the biotin-E7 peptide and the competitor peptides to Rb or p107 according to a previously described model (Kuzmic et al., 1992). Data fitting was performed using pro Fit 7 (Quantumsoft, Zurich, Switzerland).

Isothermal titration calorimetry (ITC)—Prior to ITC measurements, peptides and proteins were dialyzed overnight against a buffer containing 20 mM Tris (pH 8.0), 150 mM NaCl, and 2 mM BME at 4°C. Equilibrium dissociation constants were obtained at 19°C using a MicroCal VP-ITC system (GE Healthcare). Peptide concentrations between 300-750 μM in the syringe were injected into 25–35 μM pocket domain in the cell. A single binding site model was employed to determine the equilibrium dissociation constants. In each titration, the stoichiometry of peptide binding to pocket proteins was measured to be close to 1:1 ($n \sim 0.9$-1.1). Each experiment was performed in triplicate. Where indicated, statistical analysis of significance was performed using a two-tailed student's t-test.

Co-immunoprecipitation—Plasmids for the expression of HDAC1 mutants in mammalian cells were generated by site-directed mutagenesis following the Stratagene QuikChange mutagenesis protocol. The plasmid expressing FLAG-tagged wild-type human HDAC1 was a gift from Eric Verdin (Addgene Plasmid # 13820) (Emiliani et al., 1998). Mutant proteins were expressed from plasmid modified using site-directed mutagenesis and the oligonucleotides listed in Table S2. HCT116 cells were transfected in 10 cm plates with 8 μg plasmid and 40 μl PEI. 24 h after transfection, cells were treated with either 1 μM Palbociclib or 1 μl Nocodazole for additional 24 h. Cells were lysed with IP buffer containing (Tris pH 8.0, 0.2% Triton X, protease inhibitors (EDTA-free protease inhibitor tables, Pierce)) supplemented with 300 mM NaCl by incubation for 10 min on ice followed by direct sonication (5 times for 1 s). Lysates were cleared by centrifugation (4 °C, 10 min, 20,000 xg) and diluted with IP buffer to an NaCl concentration of 150mM. 4mg protein in 2ml IP buffer were incubated with 40μl Anti-DYKDDDDK Magnetic Agarose (Pierce)

on a rotator for 30min at 4°C. Beads were washed 5x with IP buffer/150 mM NaCl and bound proteins were eluted with 50 µl 1x Laemmli buffer at 95°C. Western blots were performed following standard protocols. The following antibodies were applied to detect RB, p107, and HDAC-FLAG: RB-C2 (Santa Cruz Biotech, sc-74562, RRID:AB_2177334), RB phospho S807 (Abcam, ab47762, RRID:AB_882296), p107-D3P3C (Cell Signaling Technology, #89798, RRID:AB_2800144), and Anti-OctA-Probe H-5 (Santa Cruz Biotech, sc-166355, RRID:AB_2017593).

Quantification and Statistical Analysis

Details of statistical analysis can be found in the methods section and figure caption. Measurements were analyzed using a two-tailed paired student's t-test and a significant difference was concluded if $p < 0.05$.

Supplementary Material

Refer to Web version on PubMed Central for supplementary material.

Acknowledgements

This work was supported by grants from the National Institutes of Health to S.M.R. (R01GM124148 and R01GM127707), Ministerio de Ciencia, Tecnología e Innovación Productiva and Deutscher Akademischer Austauschdienst (MinCyT-DAAD) to L.B.C. and T.J.G. (CyCMotif DA/16/05), and Agencia Nacional de Promoción Científica y Tecnológica (ANPCyT) Grant #PICT 2017/1924 to L.B.C. This research has received funding from the European Union's Horizon 2020 research and innovation program to L.B.C. and T.J.G. under the Marie Skłodowska-Curie grant agreement no. 778247 (IDPfun). L.B.C. is a National Research Council Investigator (CONICET, Argentina), and L.A was supported by a CONICET postdoctoral fellowship.

References

Adams PD, Afonine PV, Bunkoczi G, Chen VB, Davis IW, Echols N, Headd JJ, Hung LW, Kapral GJ, Grosse-Kunstleve RW, et al. (2010). PHENIX: a comprehensive Python-based system for macromolecular structure solution. Acta Crystallogr D Biol Crystallogr 66, 213–221. [PubMed: 20124702]

Banerjee NS, Genovese NJ, Noya F, Chien WM, Broker TR, and Chow LT (2006). Conditionally activated E7 proteins of high-risk and low-risk human papillomaviruses induce S phase in postmitotic, differentiated human keratinocytes. J Virol 80, 6517–6524. [PubMed: 16775338]

Bourgo RJ, Thangavel C, Ertel A, Bergseid J, McClendon AK, Wilkens L, Witkiewicz AK, Wang JY, and Knudsen ES (2011). RB restricts DNA damage-initiated tumorigenesis through an LXCXE-dependent mechanism of transcriptional control. Mol Cell 43, 663–672. [PubMed: 21855804]

Brehm A, Miska EA, McCance DJ, Reid JL, Bannister AJ, and Kouzarides T (1998). Retinoblastoma protein recruits histone deacetylase to repress transcription. Nature 391, 597–601. [PubMed: 9468139]

Bugge K, Brakti I, Fernandes CB, Dreier JE, Lundsgaard JE, Olsen JG, Skriver K, and Kragelund BB (2020). Interactions by Disorder - A Matter of Context. Front Mol Biosci 7, 110. [PubMed: 32613009]

Burke JR, Hura GL, and Rubin SM (2012). Structures of inactive retinoblastoma protein reveal multiple mechanisms for cell cycle control. Genes Dev 26, 1156–1166. [PubMed: 22569856]

Burkhart DL, and Sage J (2008). Cellular mechanisms of tumour suppression by the retinoblastoma gene. Nat Rev Cancer 8, 671–682. [PubMed: 18650841]

Chemes LB, Sanchez IE, and de Prat-Gay G (2011). Kinetic recognition of the retinoblastoma tumor suppressor by a specific protein target. J Mol Biol 412, 267–284. [PubMed: 21787785]

Chemes LB, Sanchez IE, Smal C, and de Prat-Gay G (2010). Targeting mechanism of the retinoblastoma tumor suppressor by a prototypical viral oncoprotein. Structural modularity, intrinsic disorder and phosphorylation of human papillomavirus E7. FEBS J 277, 973–988. [PubMed: 20088881]

Classon M, and Harlow E (2002). The retinoblastoma tumour suppressor in development and cancer. Nat Rev Cancer 2, 910–917. [PubMed: 12459729]

Coschi CH, Martens AL, Ritchie K, Francis SM, Chakrabarti S, Berube NG, and Dick FA (2010). Mitotic chromosome condensation mediated by the retinoblastoma protein is tumor-suppressive. Genes Dev 24, 1351–1363. [PubMed: 20551166]

Crisostomo L, Soriano AM, Mendez M, Graves D, and Pelka P (2019). Temporal dynamics of adenovirus 5 gene expression in normal human cells. PLoS One 14, e0211192. [PubMed: 30677073]

Davey NE, Cyert MS, and Moses AM (2015). Short linear motifs - ex nihilo evolution of protein regulation. Cell Commun Signal 13, 43. [PubMed: 26589632]

DeCaprio JA (2009). How the Rb tumor suppressor structure and function was revealed by the study of Adenovirus and SV40. Virology 384, 274–284. [PubMed: 19150725]

Defeo-Jones D, Huang PS, Jones RE, Haskell KM, Vuocolo GA, Hanobik MG, Huber HE, and Oliff A (1991). Cloning of cDNAs for cellular proteins that bind to the retinoblastoma gene product. Nature 352, 251–254. [PubMed: 1857421]

Dick FA, Goodrich DW, Sage J, and Dyson NJ (2018). Non-canonical functions of the RB protein in cancer. Nat Rev Cancer 18, 442–451. [PubMed: 29692417]

Dick FA, and Rubin SM (2013). Molecular mechanisms underlying RB protein function. Nat Rev Mol Cell Biol 14, 297–306. [PubMed: 23594950]

Dowhanick JJ, McBride AA, and Howley PM (1995). Suppression of cellular proliferation by the papillomavirus E2 protein. J Virol 69, 7791–7799. [PubMed: 7494290]

Emiliani S, Fischle W, Van Lint C, Al-Abed Y, and Verdin E (1998). Characterization of a human RPD3 ortholog, HDAC3. Proc Natl Acad Sci U S A 95, 2795–2800. [PubMed: 9501169]

Emsley P, and Cowtan K (2004). Coot: model-building tools for molecular graphics. Acta Crystallogr D Biol Crystallogr 60, 2126–2132. [PubMed: 15572765]

Evans P (2006). Scaling and assessment of data quality. Acta Crystallogr D Biol Crystallogr 62, 72–82. [PubMed: 16369096]

Fattaey AR, Helin K, Dembski MS, Dyson N, Harlow E, Vuocolo GA, Hanobik MG, Haskell KM, Oliff A, Defeo-Jones D, et al. (1993). Characterization of the retinoblastoma binding proteins RBP1 and RBP2. Oncogene 8, 3149–3156. [PubMed: 8414517]

Fera D, Schultz DC, Hodawadekar S, Reichman M, Donover PS, Melvin J, Troutman S, Kissil JL, Huryn DM, and Marmorstein R (2012). Identification and characterization of small molecule antagonists of pRb inactivation by viral oncoproteins. Chem Biol 19, 518–528. [PubMed: 22520758]

Ferreira R, Magnaghi-Jaulin L, Robin P, Harel-Bellan A, and Trouche D (1998). The three members of the pocket proteins family share the ability to repress E2F activity through recruitment of a histone deacetylase. Proc Natl Acad Sci U S A 95, 10493–10498. [PubMed: 9724731]

Gibson TJ (2009). Cell regulation: determined to signal discrete cooperation. Trends Biochem Sci 34, 471–482. [PubMed: 19744855]

Gonzalo S, Garcia-Cao M, Fraga MF, Schotta G, Peters AH, Cotter SE, Eguia R, Dean DC, Esteller M, Jenuwein T, et al. (2005). Role of the RB1 family in stabilizing histone methylation at constitutive heterochromatin. Nat Cell Biol 7, 420–428. [PubMed: 15750587]

Guiley KZ, Liban TJ, Felthousen JG, Ramanan P, Litovchick L, and Rubin SM (2015). Structural mechanisms of DREAM complex assembly and regulation. Genes Dev 29, 961–974. [PubMed: 25917549]

Harbour JW, Luo RX, Dei Santi A, Postigo AA, and Dean DC (1999). Cdk phosphorylation triggers sequential intramolecular interactions that progressively block Rb functions as cells move through G1. Cell 98, 859–869. [PubMed: 10499802]

Hassler M, Singh S, Yue WW, Luczynski M, Lakbir R, Sanchez-Sanchez F, Bader T, Pearl LH, and Mittnacht S (2007). Crystal structure of the retinoblastoma protein N domain provides insight

into tumor suppression, ligand interaction, and holoprotein architecture. Mol Cell 28, 371–385. [PubMed: 17996702]

Ivarsson Y, and Jemth P (2019). Affinity and specificity of motif-based protein-protein interactions. Curr Opin Struct Biol 54, 26–33. [PubMed: 30368054]

Jones RE, Wegrzyn RJ, Patrick DR, Balishin NL, Vuocolo GA, Riemen MW, Defeo-Jones D, Garsky VM, Heimbrook DC, and Oliff A (1990). Identification of HPV-16 E7 peptides that are potent antagonists of E7 binding to the retinoblastoma suppressor protein. J Biol Chem 265, 12782–12785. [PubMed: 2198278]

Kabsch W (2010). Integration, scaling, space-group assignment and post-refinement. Acta Crystallogr D Biol Crystallogr 66, 133–144. [PubMed: 20124693]

Kim HY, Ahn BY, and Cho Y (2001). Structural basis for the inactivation of retinoblastoma tumor suppressor by SV40 large T antigen. EMBO J 20, 295–304. [PubMed: 11226179]

Knudsen ES, Pruitt SC, Hershberger PA, Witkiewicz AK, and Goodrich DW (2019). Cell Cycle and Beyond: Exploiting New RB1 Controlled Mechanisms for Cancer Therapy. Trends Cancer 5, 308–324. [PubMed: 31174843]

Kumar M, Michael S, Alvarado-Valverde J, Meszaros B, Samano-Sanchez H, Zeke A, Dobson L, Lazar T, Ord M, Nagpal A, et al. (2021). The Eukaryotic Linear Motif resource: 2022 release. Nucleic Acids Res.

Kuzmic P, Moss ML, Kofron JL, and Rich DH (1992). Fluorescence displacement method for the determination of receptor-ligand binding constants. Anal Biochem 205, 65–69. [PubMed: 1332537]

Lai A, Lee JM, Yang WM, DeCaprio JA, Kaelin WG Jr., Seto E, and Branton PE (1999). RBP1 recruits both histone deacetylase-dependent and -independent repression activities to retinoblastoma family proteins. Mol Cell Biol 19, 6632–6641. [PubMed: 10490602]

Lee C, Chang JH, Lee HS, and Cho Y (2002). Structural basis for the recognition of the E2F transactivation domain by the retinoblastoma tumor suppressor. Genes Dev 16, 3199–3212. [PubMed: 12502741]

Lee JO, Russo AA, and Pavletich NP (1998). Structure of the retinoblastoma tumour-suppressor pocket domain bound to a peptide from HPV E7. Nature 391, 859–865. [PubMed: 9495340]

Liban TJ, Medina EM, Tripathi S, Sengupta S, Henry RW, Buchler NE, and Rubin SM (2017). Conservation and divergence of C-terminal domain structure in the retinoblastoma protein family. Proc Natl Acad Sci U S A 114, 4942–4947. [PubMed: 28439018]

Liban TJ, Thwaites MJ, Dick FA, and Rubin SM (2016). Structural Conservation and E2F Binding Specificity within the Retinoblastoma Pocket Protein Family. J Mol Biol 428, 3960–3971. [PubMed: 27567532]

Litovchick L, Florens LA, Swanson SK, Washburn MP, and DeCaprio JA (2011). DYRK1A protein kinase promotes quiescence and senescence through DREAM complex assembly. Genes Dev 25, 801–813. [PubMed: 21498570]

Litovchick L, Sadasivam S, Florens L, Zhu X, Swanson SK, Velmurugan S, Chen R, Washburn MP, Liu XS, and DeCaprio JA (2007). Evolutionarily conserved multisubunit RBL2/p130 and E2F4 protein complex represses human cell cycle-dependent genes in quiescence. Mol Cell 26, 539–551. [PubMed: 17531812]

Luo RX, Postigo AA, and Dean DC (1998). Rb interacts with histone deacetylase to repress transcription. Cell 92, 463–473. [PubMed: 9491888]

MacLellan WR, Xiao G, Abdellatif M, and Schneider MD (2000). A novel Rb- and p300-binding protein inhibits transactivation by MyoD. Mol Cell Biol 20, 8903–8915. [PubMed: 11073990]

Magnaghi-Jaulin L, Groisman R, Naguibneva I, Robin P, Lorain S, Le Villain JP, Troalen F, Trouche D, and Harel-Bellan A (1998). Retinoblastoma protein represses transcription by recruiting a histone deacetylase. Nature 391, 601–605. [PubMed: 9468140]

Manning AL, Longworth MS, and Dyson NJ (2010). Loss of pRB causes centromere dysfunction and chromosomal instability. Genes Dev 24, 1364–1376. [PubMed: 20551165]

Miyake S, Sellers WR, Safran M, Li X, Zhao W, Grossman SR, Gan J, DeCaprio JA, Adams PD, and Kaelin WG Jr. (2000). Cells degrade a novel inhibitor of differentiation with E1A-like properties upon exiting the cell cycle. Mol Cell Biol 20, 8889–8902. [PubMed: 11073989]

Morris EJ, and Dyson NJ (2001). Retinoblastoma protein partners. Adv Cancer Res 82, 1–54. [PubMed: 11447760]

Mulligan G, and Jacks T (1998). The retinoblastoma gene family: cousins with overlapping interests. Trends Genet 14, 223–229. [PubMed: 9635405]

Palopoli N, Gonzalez Foutel NS, Gibson TJ, and Chemes LB (2018). Short linear motif core and flanking regions modulate retinoblastoma protein binding affinity and specificity. Protein Eng Des Sel 31, 69–77. [PubMed: 29370437]

Pflum MK, Tong JK, Lane WS, and Schreiber SL (2001). Histone deacetylase 1 phosphorylation promotes enzymatic activity and complex formation. J Biol Chem 276, 47733–47741. [PubMed: 11602581]

Prestel A, Wichmann N, Martins JM, Marabini R, Kassem N, Broendum SS, Otterlei M, Nielsen O, Willemoes M, Ploug M, et al. (2019). The PCNA interaction motifs revisited: thinking outside the PIP-box. Cell Mol Life Sci 76, 4923–4943. [PubMed: 31134302]

Rubin SM (2013). Deciphering the retinoblastoma protein phosphorylation code. Trends Biochem Sci 38, 12–19. [PubMed: 23218751]

Sanidas I, Morris R, Fella KA, Rumde PH, Boukhali M, Tai EC, Ting DT, Lawrence MS, Haas W, and Dyson NJ (2019). A Code of Mono-phosphorylation Modulates the Function of RB. Mol Cell 73, 985–1000 e1006. [PubMed: 30711375]

Sherr CJ, and McCormick F (2002). The RB and p53 pathways in cancer. Cancer Cell 2, 103–112. [PubMed: 12204530]

Singh M, Krajewski M, Mikolajka A, and Holak TA (2005). Molecular determinants for the complex formation between the retinoblastoma protein and LXCXE sequences. J Biol Chem 280, 37868–37876. [PubMed: 16118215]

Sun Y, Stine JM, Atwater DZ, Sharmin A, Ross JB, and Briknarova K (2015). Structural and functional characterization of the acidic region from the RIZ tumor suppressor. Biochemistry 54, 1390–1400. [PubMed: 25640033]

Talluri S, and Dick FA (2012). Regulation of transcription and chromatin structure by pRB: here, there and everywhere. Cell Cycle 11, 3189–3198. [PubMed: 22895179]

Teilum K, Olsen JG, and Kragelund BB (2021). On the specificity of protein-protein interactions in the context of disorder. Biochem J 478, 2035–2050. [PubMed: 34101805]

Topacio BR, Zatulovskiy E, Cristea S, Xie S, Tambo CS, Rubin SM, Sage J, Koivomagi M, and Skotheim JM (2019). Cyclin D-Cdk4,6 Drives Cell-Cycle Progression via the Retinoblastoma Protein's C-Terminal Helix. Mol Cell 74, 758–770 e754. [PubMed: 30982746]

Trimarchi JM, and Lees JA (2002). Sibling rivalry in the E2F family. Nat Rev Mol Cell Biol 3, 11–20. [PubMed: 11823794]

Vagin A, and Teplyakov A (2010). Molecular replacement with MOLREP. Acta Crystallogr D Biol Crystallogr 66, 22–25. [PubMed: 20057045]

van den Heuvel S, and Dyson NJ (2008). Conserved functions of the pRB and E2F families. Nat Rev Mol Cell Biol 9, 713–724. [PubMed: 18719710]

Winn MD, Ballard CC, Cowtan KD, Dodson EJ, Emsley P, Evans PR, Keegan RM, Krissinel EB, Leslie AG, McCoy A, et al. (2011). Overview of the CCP4 suite and current developments. Acta Crystallogr D Biol Crystallogr 67, 235–242. [PubMed: 21460441]

Winter G (2010). xia2: an expert system for macromolecular crystallography data reduction. J Appl Crystallogr 43, 186–190.

Xiao B, Spencer J, Clements A, Ali-Khan N, Mittnacht S, Broceno C, Burghammer M, Perrakis A, Marmorstein R, and Gamblin SJ (2003). Crystal structure of the retinoblastoma tumor suppressor protein bound to E2F and the molecular basis of its regulation. Proc Natl Acad Sci U S A 100, 2363–2368. [PubMed: 12598654]

Zhang HS, Gavin M, Dahiya A, Postigo AA, Ma D, Luo RX, Harbour JW, and Dean DC (2000). Exit from G1 and S phase of the cell cycle is regulated by repressor complexes containing HDAC-Rb-hSWI/SNF and Rb-hSWI/SNF. Cell 101, 79–89. [PubMed: 10778858]

Zitterbart R, Berger N, Reimann O, Noble GT, Ludtke S, Sarma D, and Seitz O (2021). Traceless parallel peptide purification by a first-in-class reductively cleavable linker system featuring a safety-release. Chem Sci 12, 2389–2396. [PubMed: 34164003]

Highlights

- Binding data reveals wide range of affinities of LxCxE motifs for Rb proteins
- X-ray structures explain the importance of residues outside the core motif
- Sequence differences in Rb and p107 at the LxCxE-binding site determine specificity

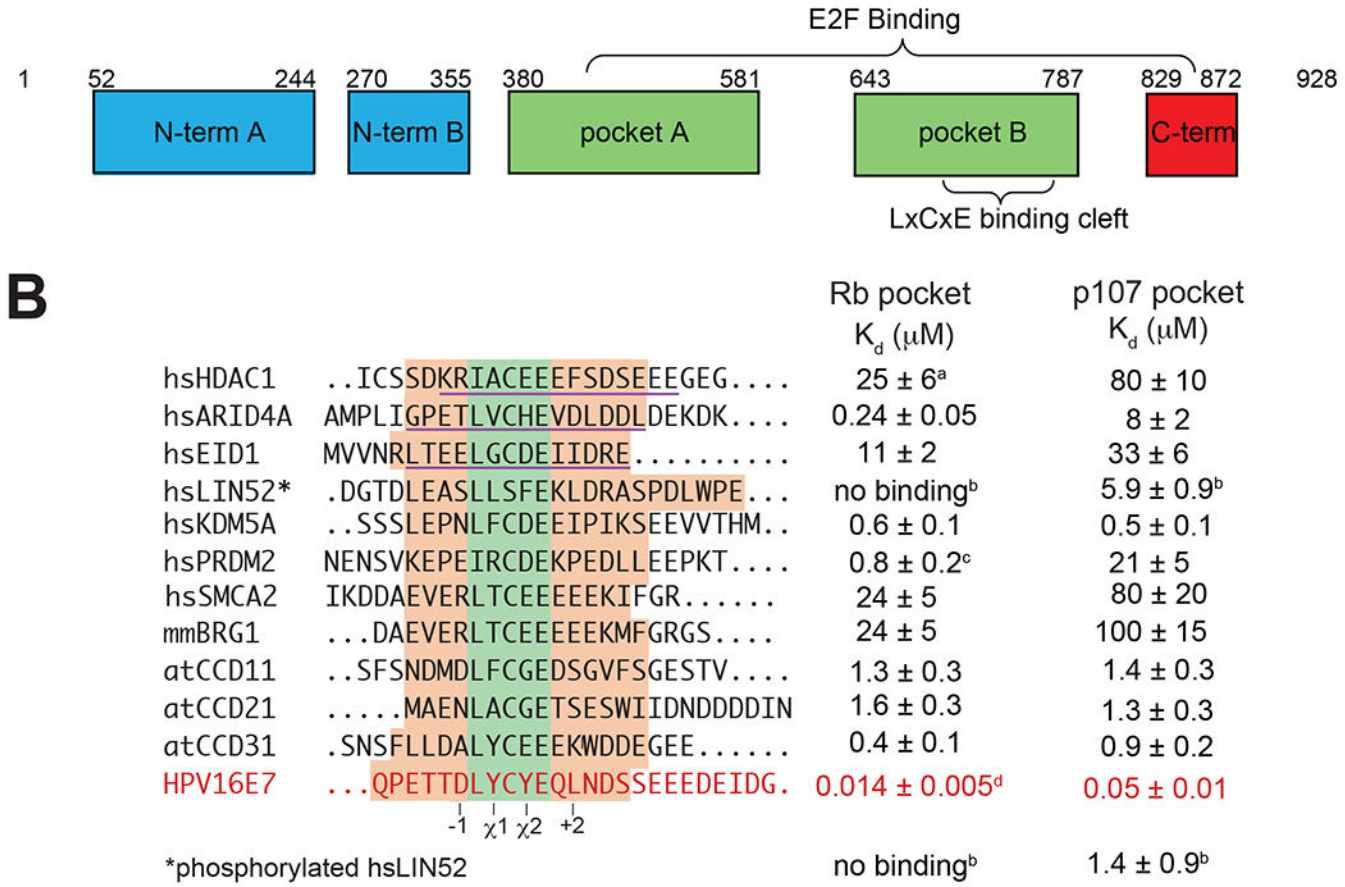

Figure 1. Affinity measurements of LxCxE peptides for Rb and p107.

(A) Schematic diagram of the domain organization of Rb. A similar domain architecture is observed in p107 and p130. (B) AlphaScreen affinity measurements of cellular LxCxE peptides and comparison to the viral E7 peptide. In the sequence alignment, the peptide sequences used for affinity studies are colored peach, the core LxCxE motif is colored green, and the peptide sequence used in structural studies is underlined. The position of variable amino acids relative to the core (−1, +2) and the wild-card positions in the core motif (χ^1 and χ^2) are labeled. hs is Homo sapiens, mm is Mus musculus, and at is Arabidopsis thaliana. [a]Measured here and also reported as Kd = 10 ± 3 μM in (Singh et al., 2005). [b]Reported in (Guiley et al., 2015). [c]Measured here and also reported as Kd = 0.64 ± 0.07 μM in (Sun et al., 2015). [d]Measured here and also reported as Kd = 0.005 ± 0.001 μM in (Chemes et al., 2011).

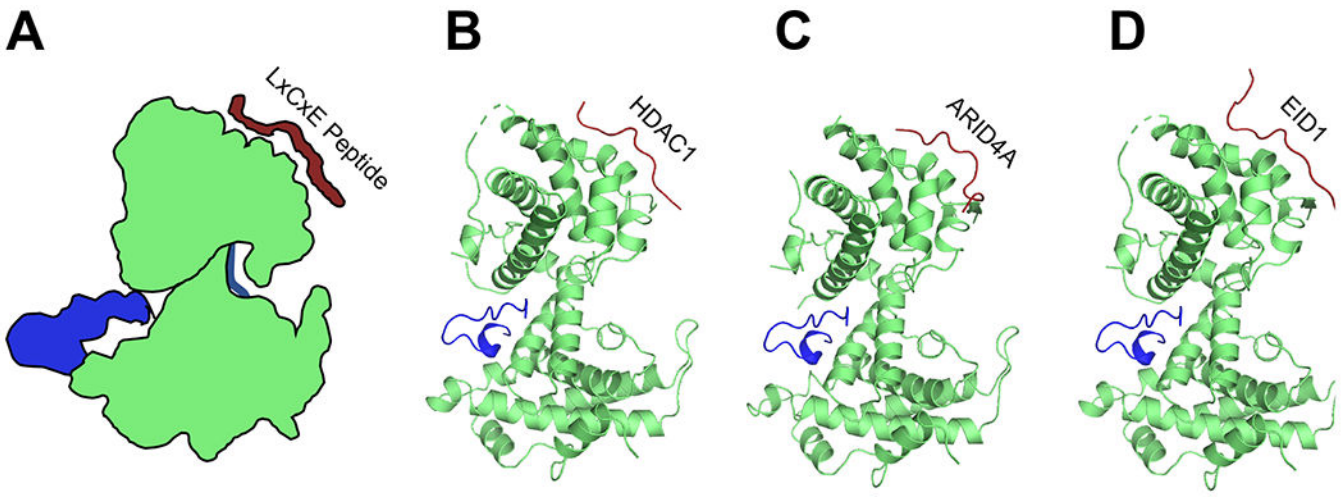

Figure 2. Structures of P107ΔL with cellular LxCxE peptides.

(A) Schematic of the architecture of the p107 pocket domain showing the E2F and LxCxE binding sites. (B, C, and D) Ribbon models of p107ΔL pocket domain with human HDAC1, ARID4A, and EID1 LxCxE motif peptides. The pocket domain is shown in green, and the E2F and LxCxE peptides are shown in blue and red, respectively. The E2F peptide shown here is from PDB: 1N4M and is superposed to model the different locations of the binding sites.

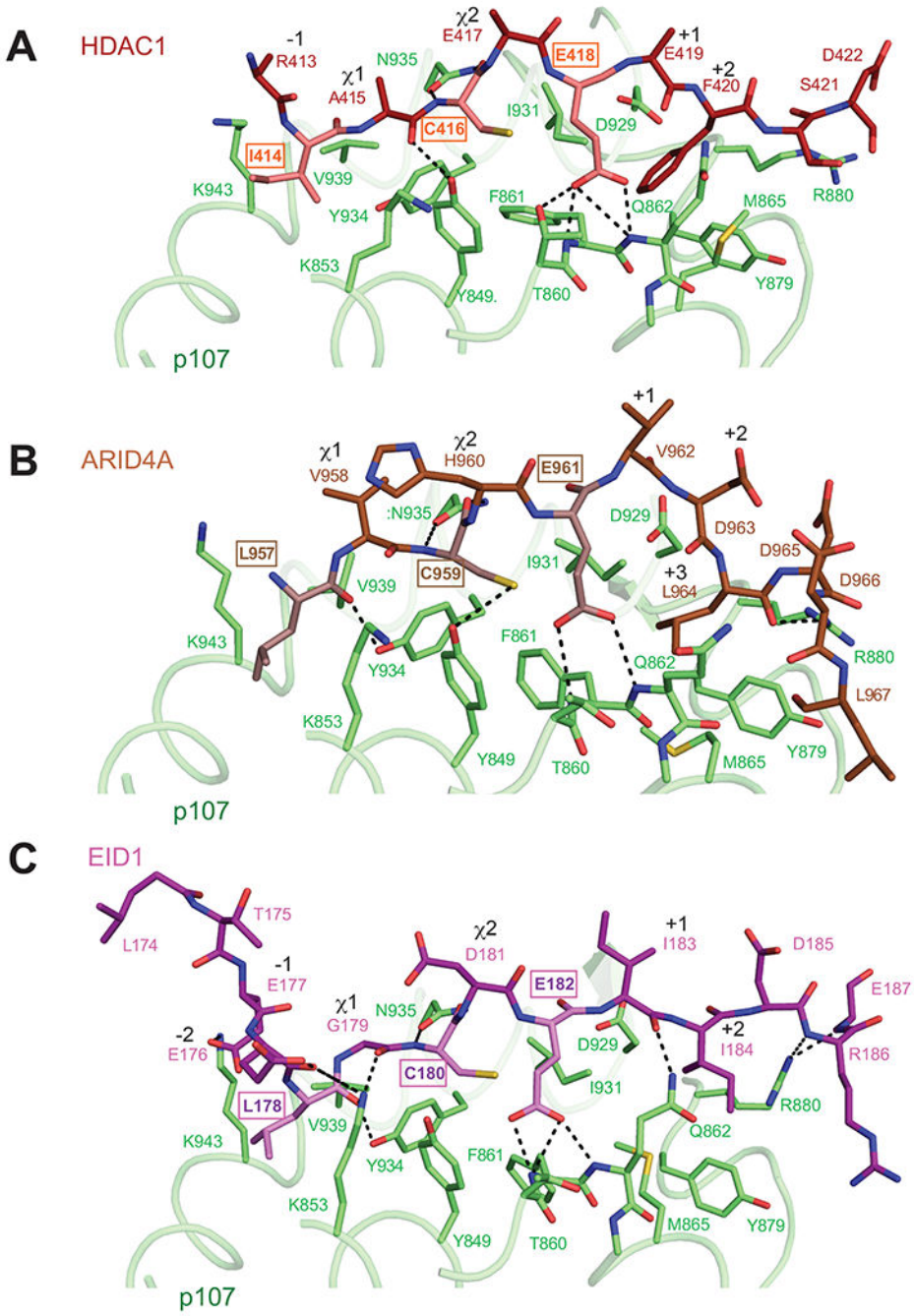

Figure 3. Comparison of binding interactions made by cellular LxCxE peptides.

p107ΔL pocket domain in complex with peptides from (A) HDAC1, (B) ARID4A, and (C) EID1. The core LCE motif residues are underlined.

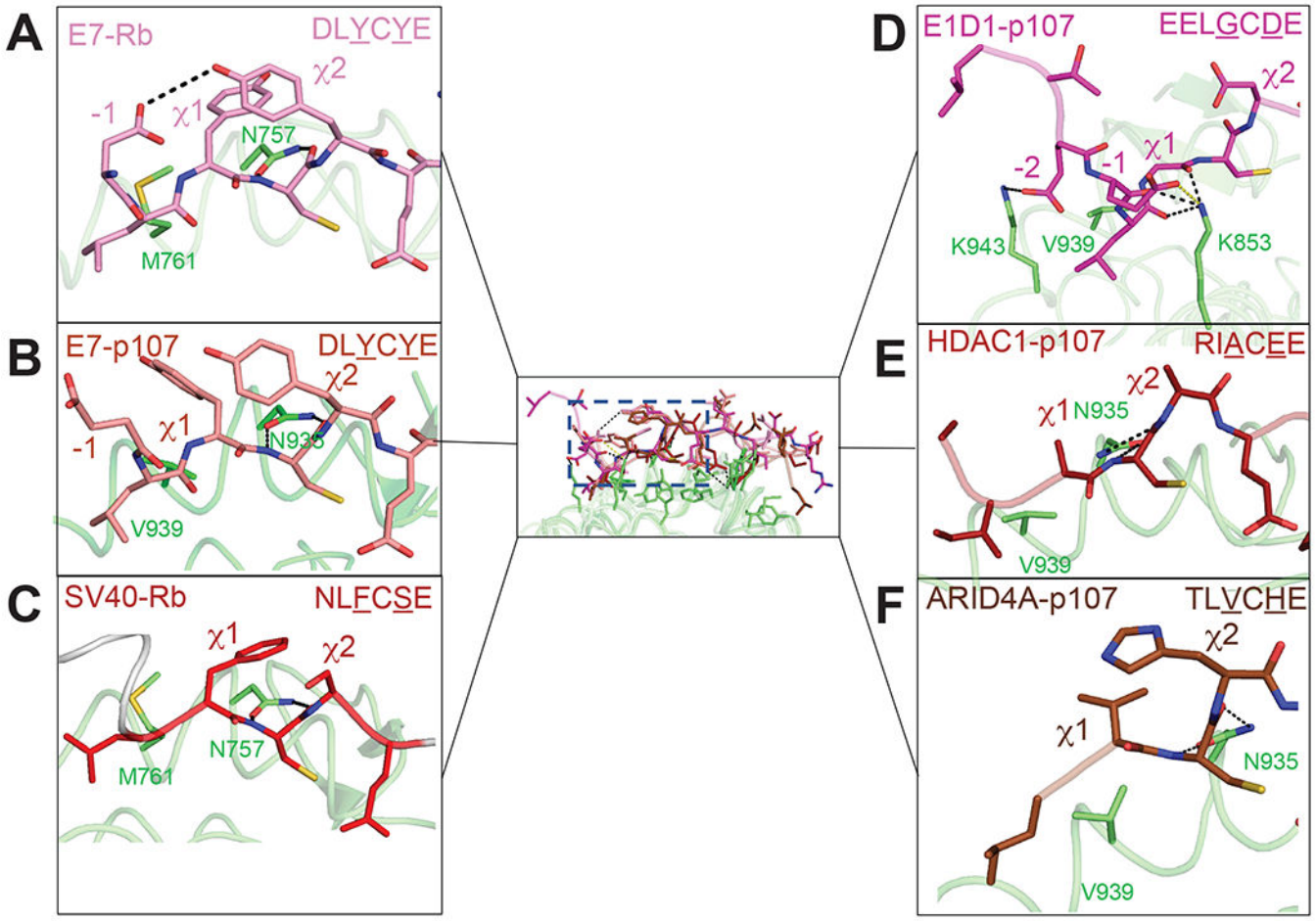

Figure 4. Interactions N-terminal to the core LXCXE motif and position of wild-card residues.

The aligned structures of (A) E7-Rb, (B) E7-p107, (C) SV40-Rb, (D) EID1-p107, (E) HDAC1-p107, and (F) ARI4DA-p107. Peptides are shown overlaid in the middle panel and are separated in the peripheral panels to show the individual conformations of the wild-card sidechains (χ^1 and χ^2, underlined in sequence) and N-terminal (−1, −2, etc.) acidic residues.

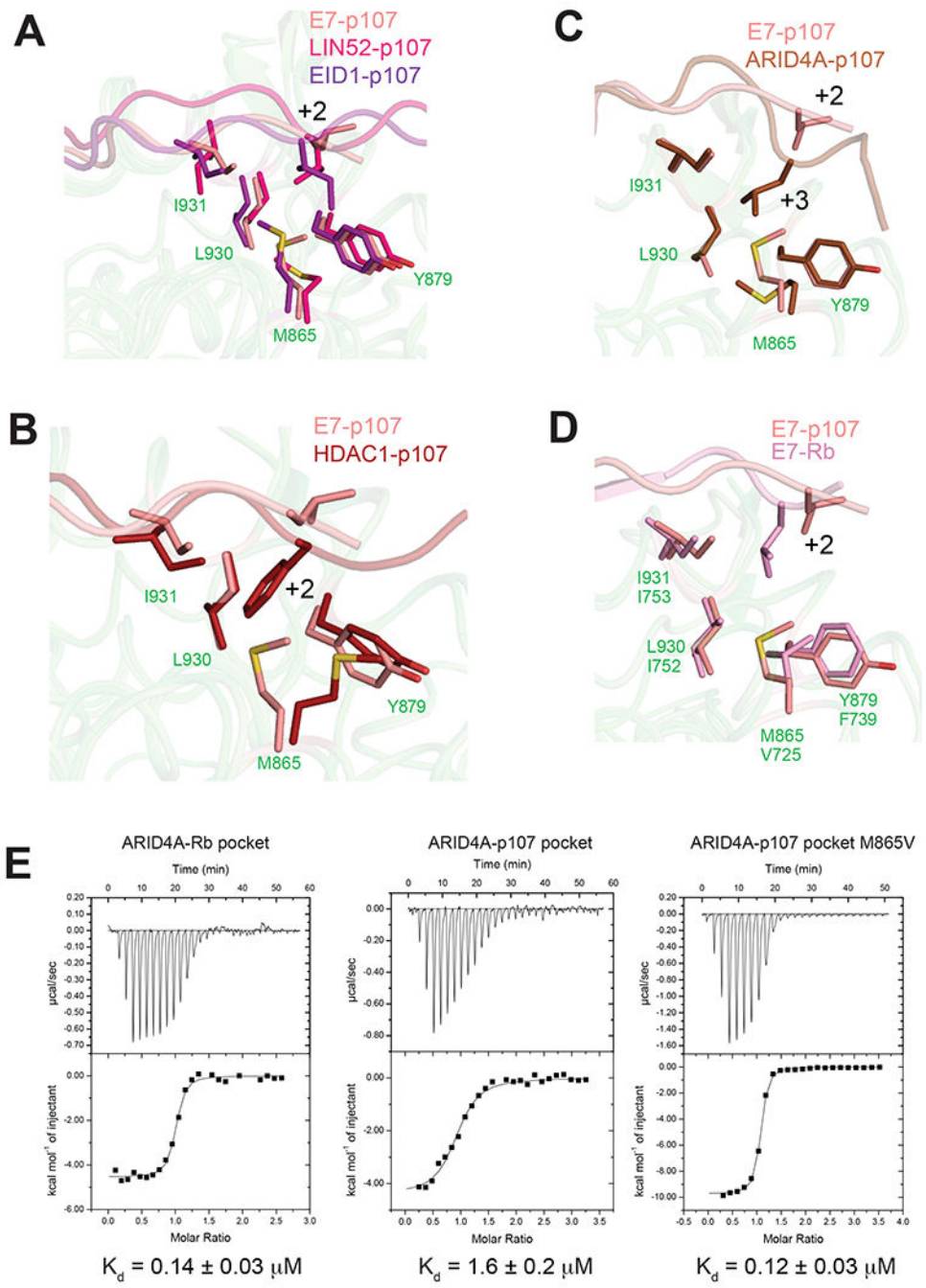

Figure 5. Flexibility in accommodating a +2/+3 hydrophobic sidechain.

(A) Similar sidechains in the +2 position of E7, LIN52, and EID1 are oriented differently within the broad hydrophobic pocket of p107. (B) HDAC1 inserts its +2 phenylalanine deeper into the pocket, and M865 in p107 changes its position to avoid steric clash. (C) The +3 leucine of ARID4A is inserted deeper into the core relative to the E7 +2 leucine because of the angle of the main chain. M865 changes its position to accommodate the deeper leucine sidechain. (D) The V725 present in Rb at the same position as p107 M865 allows deeper insertion of the +2/+3 sidechain into the pocket without potential steric clash. (E)

ITC measurements of ARID4A peptide binding to the indicated pocket domain construct. The reported Kd is the average of three replicates with the standard deviation reported as error.

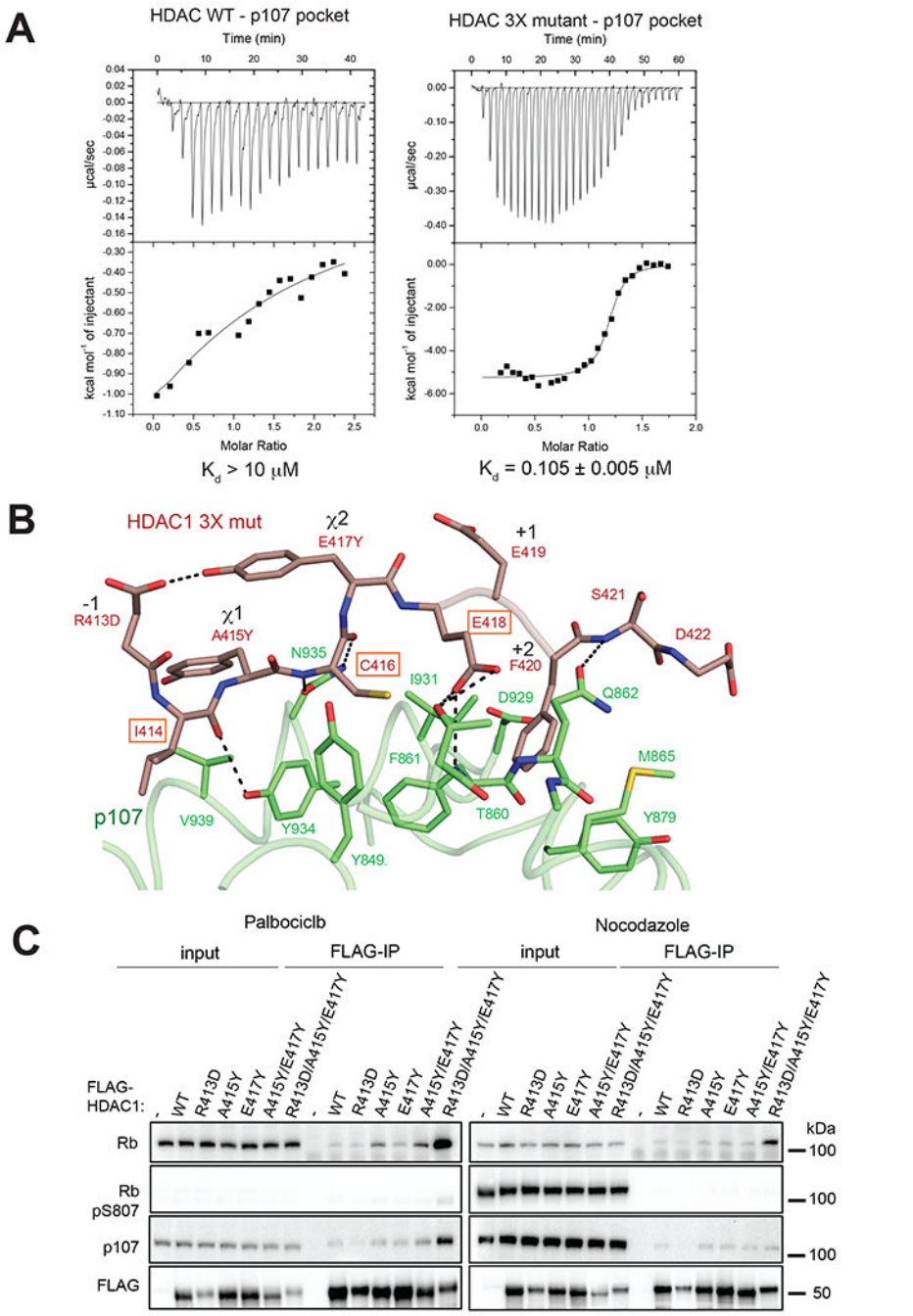

Figure 6. Mutation of the wild card residues and −1 acidic residue result in a high affinity HDAC1 interaction.

(A) ITC data of HDAC1 3X mutant binding to the p107 pocket domain. (B) Crystal structure of HDAC1 3X bound to the pocket domain of p107. Mutations mimicking (D413, Y415 and Y417) the HPV16 E7 peptide were introduced into the HDAC1 LXCXE motif and show similar orientation as in the E7 peptide structures. (C) HCT116 cells transfected with the indicated HDAC1 construct were treated with drug for 24hrs prior to lysis, and immunoprecipitation was performed with an anti-Flag antibody.

Table 1.

X-ray diffraction data and model refinement summary

	p107-ARID4A	p107-EID1	p107-HDAC1	p107-HDAC1-3X
PDB Id.	7SMC	7SMD	7SME	7SMF
Data collection				
Beam line	APS 23(IDD)	APS 23(IDD)	APS 23(IDD)	APS 23(IDD)
Space group	P1	$C_1$21	$C_1$21	P1
Unit cell dimensions a,b,c (Å), α, β, γ (°)	62.8, 62.9, 71.2 69.8, 76, 74.3	98.7, 75.8, 71.9, 90, 108.4, 90	99.9, 75.1, 71.7, 90, 109.8, 90	63.1, 63.3, 83.3, 85.9, 68.4, 73.9
Resolution Range (Å)	47.11 - 2.70 (2.83 - 2.7)	33.92-2.15 (2.22-2.15)	46.98-2.64 (2.76-2.64)	39.29-3.00 (3.18-3.00)
Wavelength (Å)	1.0332	1.033	1.033	1.033
Total observations	95391 (10825)	176053 (15109)	117829 (15220)	42431 (6502)
Unique reflections	26604 (3491)	27480 (2385)	14817 (1937)	21589 (3425)
Completeness (%)	99.3 (97.4)	99.9 (99.9)	99.6 (98.4)	93.5 (91.8)
R_{merge}	16.3 (52.7)	7.4 (96.3)	18.9 (63.8)	25.1(73.8)
<I/σ>	5.3 (2.0)	11.5 (1.8)	7.8 (3.8)	3.1(1.3)
CC1/2	0.97 (0.64)	0.99 (0.70)	0.99 (0.89)	0.81(0.64)
Redundancy	3.6 (3.1)	6.4 (6.3)	8.0 (7.9)	2.0(1.9)
Refinement				
R_{work} %/ R_{free} %	23.8 (29.7)	22.7 (25.9)	22.6 (27.4)	23.7 (30.0)
Number of non-hydrogen atoms	5750	2951	2885	5790
Protein	35704	2882	2842	5728
Water	31	59	33	42
B-factor (Wilson) (Å^2)	46	54.1	57.6	40.9
RMSD Bond length (Å)	0.01	0.013	0.013	0.014
RMSD Bond angle (°)	1.69	1.84	1.96	2.0
Ramachandran favored(%)/ Ramachandran outliers (%)	96.06/0.15	97.4/0.0	96.49/0.0	90.79/0.58

*Values in parenthesis are for higher resolution shell.

Table 2.

Summary of ITC binding measurements.

Example raw data traces for each measurement are shown in Figure S4. p values were calculated between mutant and corresponding wild-type experiments using a two-tailed t-test and indicated at the right of the mutant experiment as follows: N.S. (not significant, $p > 0.05$),

Peptide	Pocket Domain	K_d (μM)	
EID1	Rb	6 ± 3	
EID1 E176R/E177R	Rb	9 ± 4	N.S.
EID1	p107	7 ± 5	
EID1 E176R/E177R	p107	14 ± 5	N.S.
EID1	Rb K713A/K765A	no detectable affinity	
EID1	p107 K853A/K943A	no detectable affinity	
ARID4A	Rb	0.14 ± 0.03	
ARID4A E955R	Rb	0.5 ± 0.1	*
ARID4A	p107	1.6 ± 0.2	
ARID4A E955R	p107	2.3 ± 0.5	N.S.
E7	Rb	0.06 ± 0.01	
E7	Rb N757A	no detectable affinity	
E7	p107	0.10 ± 0.03	
E7	p107 N935A	no detectable affinity	
ARID4A	p107 M865V	0.12 ± 0.03	**
ARID4A	p107 V939M	0.33 ± 0.06	*
HDAC	p107	>10	
HDAC R413D/A415Y/E417Y	p107	0.105 ± 0.005	
HDAC R413D/A415Y/E417Y	Rb	0.03 ± 0.02	
EID1 G179Y/D181Y	Rb	0.17 ± 0.08	
EID1 G179Y/D181Y	p107	0.25 ± 0.06	

* $p < 0.05$, and

** $p < 0.01$.

Key resources table

REAGENT or RESOURCE	SOURCE	IDENTIFIER
Antibodies		
RB-C2	Santa Cruz Biotech	sc-74562; RRID:AB_2177334
RB phospho S807	Abcam	ab47762; RRID:AB_882296
p107-D3P3C	Cell Signaling Technology	#89798; RRID:AB_2800144
Anti-OctA-Probe H-5	Santa Cruz Biotech	sc-166355; RRID:AB_2017593
Bacterial and virus strains		
E. coli BL21(DE3)	New England Biolabs	Cat#: C2527
Chemicals, peptides, and recombinant proteins		
Synthetic peptides for AlphaScreen	Belyntic GmbH	See Table S1
Synthetic peptides for X-ray crystallography	Genscript Biotech	See Figure 1 and Table S1
Deposited data		
p107-ARID4A structure	This paper	PDB: 7SMC
p107-EID1 structure	This paper	PDB: 7SMD
p107-HDAC1 structure	This paper	PDB: 7SME
p107-HDAC1-3X structure	This paper	PDB: 7SMF
Experimental models: Cell lines		
HCT116	ATCC	ATCC#: CCL-247
Oligonucleotides		
See Table S2 for synthetic oligonucleotides used for site-directed mutagenesis	This paper	N/A
Recombinant DNA		
FLAG-HDAC1 (human)	Emiliani et al., 1998	Addgene Plasmid # 13820
p107 pocket domain	Guiley et al., 2015	Request from lead contact
Rb pocket domain	Guiley et al., 2015	Request from lead contact
Software and algorithms		
XDS	Kabsch, 2010	https://xds.mr.mpg.de
XIA2	Winter, 2010	https://xia2.github.io
AIMLESS	Evans, 2006	https://www.ccp4.ac.uk
CCP4 program suite	Winn et al., 2011	https://www.ccp4.ac.uk
MOLREP	Vagin and Teplyakov, 2010	https://www.ccp4.ac.uk
COOT	Emsley and Cowtan, 2004	https://www.ccp4.ac.uk
Phenix	Adams et al., 2010	http://www.phenix-online.org
proFit7	Quantumsoft, Zurich, Switzerland	https://www.quansoft.com